Intermodel Spread in Indian Ocean Basin Mode Simulation: Roles of Indian Ocean Winds and Pacific Cold Tongue

Wenping Jiang[a,b,c], Jin-Yi Yu[c], Xiangzhou Song[a,b], Mengyan Chen[d], Gang Huang[e,f], Ping Huang[e], Yong-Fu Lin[g], Yunlong Ji[b]

[a]Key Laboratory of Marine Hazards Forecasting, Ministry of Natural Resources (MNR), Hohai University, Nanjing, China.

[b]College of Oceanography, Hohai University, Nanjing, China

[c]Department of Earth System Science, University of California, Irvine, CA

[d]State Key Laboratory of Tropical Oceanography, South China Sea Institute of Oceanology, Chinese Academy of Sciences, Guangzhou, China.

[e]National Key Laboratory of Earth System Numerical Modeling and Application, Institute of Atmospheric Physics, Chinese Academy of Sciences, Beijing, China.

[f]University of Chinese Academy of Sciences, Beijing, China.

[g]Research Center for Critical Issues, Academia Sinica, Taipei, Taiwan.

Corresponding author:

Wenping Jiang, jiangwenping@hhu.edu.cn;

Jin-Yi Yu, jyyu@uci.edu

Early Online Release: This preliminary version has been accepted for publication in *Journal of Climate*, may be fully cited, and has been assigned DOI 10.1175/JCLI-D-25-0438.1. The final typeset copyedited article will replace the EOR at the above DOI when it is published.

ABSTRACT

The Indian Ocean Basin Mode (IOBM) is a major component of interannual sea surface temperature (SST) variability in the tropical Indian Ocean and acts as an atmospheric–oceanic bridge extending El Niño–Southern Oscillation (ENSO)'s climate influence into the boreal summer of its decay phase—known as the capacitor effect. Despite advancements, state-of-the-art climate models continue to show systematic biases in simulating the IOBM during ENSO decay summers. Analyzing historical simulations from 56 models in phase 5 and 6 of the Coupled Models Intercomparison Project (CMIP5/6), this study identifies two dominant modes of intermodel spread in IOBM simulations: an Indian Ocean Dipole (IOD)-like mode linked to climatological easterly wind biases over the equatorial Indian Ocean, and an eastern Indian Ocean (EIO)-centered mode associated with equatorial Pacific cold tongue biases. The IOD-like spread pattern arises from easterly wind biases that weaken SST–thermocline coupling in the southwestern Indian Ocean, suppressing IOBM amplitude. The EIO-centered pattern stems from cold tongue biases that shift ENSO anomalies westward, altering EIO SSTs through Indo-Pacific interactions. Using statistical relationships between the spread modes and historical mean-state biases, we refine CMIP5/6 projections of the IOBM and its capacitor effect under warming, revealing a stronger and more consistent enhancement than previously estimated. These findings highlight the role of background climatological wind and SST biases in shaping model spread and underscore the importance of improving Indo-Pacific mean-state simulations for more reliable IOBM representation and future climate projections.

Accepted for publication in *Journal of Climate*. DOI 10.1175/JCLI-D-25-0438.1.

SIGNIFICANCE STATEMENT

This study investigates why climate models struggle to simulate the Indian Ocean Basin Mode (IOBM), a key feature that helps extend El Niño's climate influence into the summer following its peak. Analyzing historical simulations from 56 models in phase 5 and 6 of the Coupled Models Intercomparison Project (CMIP5/6), we identify two main sources of model disagreement: biases in tropical Indian Ocean winds and Pacific cold tongue sea surface termperatures. These mean-state biases not only distort the simulated IOBM but also weaken projections of the "capacitor effect", in which the IOBM enables the Indian Ocean to relay El Niño's influence. By correcting for these biases, we find that future IOBM responses and associated climate impacts may be stronger than previously thought, highlighting the need to reduce background biases in climate models.

KEYWORDS: Indian–Pacific Ocean interactions; Indian Ocean Basin Mode; Intermodel spread; CMIP5/CMIP6; ENSO; Indian Ocean Dipole; Cold tongue bias; Capacitor effect

Accepted for publication in *Journal of Climate*. DOI 10.1175/JCLI-D-25-0438.1.

1. Introduction

The Indian Ocean Basin Mode (IOBM) is a dominant mode of sea surface temperature (SST) variability in the tropical Indian Ocean, characterized by basin-wide SST anomalies of a single sign (Alexander et al. 2002; Klein et al. 1999; Schott et al. 2009). The IOBM is closely linked to El Niño–Southern Oscillation (ENSO) and typically develops during the ENSO mature phase in winter, peaks in the following spring, and persists into the summer of the ENSO decay phase (Alexander et al. 2002; Du et al. 2009; Lau and Nath 2003; Schott et al. 2009). By "storing" delayed oceanic and atmospheric adjustments, the IOBM extends climate influences of ENSO even after ENSO has dissipated. This delayed impact, commonly referred to as the Indian Ocean capacitor effect (Xie et al. 2009; Yang et al. 2007, 2010), plays a critical crucial role in allowing ENSO events to influence the East Asian summer monsoon, the western Pacific subtropical high, and other regional climate patterns (Huang et al. 2011; Qu and Huang 2012a,b; Hu et al. 2013; Xie et al. 2009).

Several mechanisms have been proposed to explain IOBM generation. A key driver is the atmospheric bridge mechanism (Alexander et al. 2002; Klein et al. 1999; Lau and Nath 1996), through which anomalous convection over the central-eastern Pacific during El Niño alters Walker circulation and induces descending motion and anticyclonic wind anomalies over the tropical Indian Ocean. The wind anomalies reduce evaporative cooling and net surface latent heat flux, leading to widespread SST warming across the basin. In addition to this remote atmospheric forcing, oceanic processes within the Indian Ocean also play an important role in shaping the IOBM evolution. Downwelling Rossby waves generated by anomalous easterlies can propagate westward, deepen the thermocline, and induce warm SST anomalies in the southwestern Indian Ocean (Masumoto and Meyers 1998; Xie et al. 2002; Chowdary and Gnanaseelan 2007; Chakravorty et al. 2014). The resulting warm anomalies intensify local convection during boreal spring and trigger an antisymmetric cross-equatorial wind pattern across the equator, which weakens the southwest monsoon and reinforces warming in the northern Indian Ocean into the El Niño decay summers through a positive wind–evaporation–SST (WES) feedback (Du et al. 2009; Wu et al. 2008). Moreover, the basin-wide SST warming can further feed back to the atmosphere through a Matsuno–Gill-type response, prolonging ENSO's influence into the subsequent summer and affecting the Asian monsoon system (Yang et al. 2007, 2010; Xie et al. 2009, 2016). Collectively, these studies indicate that the IOBM arises from the combined effects of remote ENSO forcing, local oceanic dynamics, and air–sea coupled feedbacks within the Indian Ocean.

Accepted for publication in *Journal of Climate*. DOI 10.1175/JCLI-D-25-0438.1.

Accurately simulating the Indian Ocean Basin Mode (IOBM) is essential for reliable predictions of the Indian Ocean capacitor effect and, consequently, the summer climate over Asia and the western Pacific. However, state-of-the-art coupled climate models still exhibit significant biases in representing the IOBM during ENSO decay summers (Du et al. 2013; Tao et al. 2016). Du et al. (2013) found that nearly half of the phase 5 of the Coupled Models Intercomparison Project (CMIP5) models fail to capture the observed IOBM properties. Previous studies have highlighted climatological easterly wind biases over the equatorial Indian Ocean as a potential cause of model deficiencies in simulating the IOBM, as these biases can deepen the thermocline in the southwestern Indian Ocean and diminish the thermocline–SST coupling there, thereby reducing the IOBM amplitude (Li et al. 2015; Zheng et al. 2016). In addition, climatological easterly wind biases can weaken the zonal thermocline gradient along the equator, thereby enhancing the Bjerknes feedback and shifting Indian Ocean SST variability toward a more positive IOD-like pattern (Cai et al. 2011; Cai and Cowan 2013; Weller and Cai 2013), which can disrupt the basin-wide SST anomaly pattern characteristic of the IOBM.

Moreover, since the IOBM is closely linked to ENSO, biases in simulated ENSO are also likely to influence its representation. Tao et al. (2016) found that unrealistic SST anomalies in the western Pacific associated with modeled ENSO impede the accurate simulation of both the IOBM and its capacitor effect during ENSO-decay summers in CMIP3 and CMIP5 models. Subsequent studies have proposed that the excessive westward extension and slower decay of ENSO-related SST anomalies in many climate models are associated with an overly strong climatological cold tongue bias in the equatorial Pacific (Jiang et al. 2017, 2021; Tao et al. 2018). Therefore, this Pacific SST mean-state bias may also contribute to biases in IOBM simulations.

Although previous studies have shown that the overall performance of CMIP5 models in simulating IOBM is better than that of CMIP3 models (Tao et al. 2016), it remains unclear whether CMIP6 models offer further improvements over CMIP5. Moreover, the root causes of IOBM biases—whether arising from the simulated mean state of the Indian Ocean, the Pacific Ocean, or both—and their relative contributions remain unresolved. These questions call for a systematic and comprehensive analysis. In this study, we conduct an intermodel empirical orthogonal function (EOF) analysis using outputs from 27 CMIP5 models and 29 CMIP6 models to identify the sources of model biases in IOBM simulations across the two most recent

Accepted for publication in *Journal of Climate*. DOI 10.1175/JCLI-D-25-0438.1.

generations of CMIP models. We also explore how these biases may influence future projections of the Indian Ocean capacitor effect under global warming scenarios.

The rest of the paper is organized as follows. Section 2 is a brief description of the model datasets and methods used in this study. Section 3 evaluates the IOBM simulation in CMIP5 and CMIP6 models. Section 4 investigates the leading patterns of intermodel spread in IOBM simulation during ENSO decay summers and their origins. Section 5 examines how observationally constrained corrections to key biases affect future projections of the Indian Ocean capacitor effect. Section 6 presents a summary of the main findings.

2. Data and Methods

a. Observation and Model Data

We analyze monthly outputs from the historical simulations of 27 CMIP5 models (Taylor et al. 2012) and 29 CMIP6 models (Eyring et al. 2016) over the period 1979–2005. For future projections, we use data from the RCP8.5 experiments in CMIP5 and the SSP5-8.5 experiments in CMIP6 for the period 2070–2096. The list of models used in this study is provided in Table 1. The variables analyzed include monthly mean SST, oceanic potential temperature, precipitation, latent heat flux, wind and troposphere temperature in historical simulations and monthly mean SST, precipitation, wind and troposphere temperature in future warming projections.

Reanalysis and observational datasets for the period 1979–2005 are used as a reference. The data used include monthly mean SST from the Extended Reconstructed SST, version 5 (ERSST. V5) (Huang et al. 2017); ocean potential temperature data from the Simple Ocean Data Assimilation version 2.2.4 (SODA_2.2.4) (Carton and Giese 2008); and winds from the National Centers for Environment Prediction–National Center for Atmospheric Research (NCEP–NCAR) reanalysis (Kalnay et al. 1996). All the model outputs and observational datasets are interpolated onto the same 2.5°×2.5° grid before analysis.

No.	CMIP5	No.	CMIP6
M1	ACCESS1-0	M28	BCC-CSM2-MR
M2	ACCESS1-3	M29	BCC-ESM1
M3	bcc-csm1-1-m	M30	CAMS-CSM1-0
M4	bcc-csm1-1	M31	CanESM5
M5	BNU-ESM	M32	CESM2-WACCM
M6	CanESM2	M33	CESM2

Accepted for publication in *Journal of Climate*. DOI 10.1175/JCLI-D-25-0438.1.

M7	CCSM4	M34	CNRM-CM6-1
M8	CESM1-CAM5	M35	CNRM-ESM2-1
M9	CMCC-CM	M36	E3SM-1-0
M10	CNRM-CM5	M37	EC-Earth3-Veg
M11	CSIRO-Mk3-6-0	M38	EC-Earth3
M12	FGOALS-g2	M39	FGOALS-f3-L
M13	GFDL-CM3	M40	GFDL-CM4
M14	GFDL-ESM2G	M41	GFDL-ESM4
M15	GFDL-ESM2M	M42	GISS-E2-1-G
M16	GISS-E2-H	M43	GISS-E2-1-H
M17	GISS-E2-R	M44	HadGEM3-GC31-LL
M18	HadGEM2-ES	M45	INM-CM4-8
M19	IPSL-CM5A-LR	M46	INM-CM5-0
M20	IPSL-CM5A-MR	M47	IPSL-CM6A-LR
M21	MIROC-ESM	M48	MIROC-ES2L
M22	MIROC5	M49	MIROC6
M23	MPI-ESM-LR	M50	MPI-ESM1-2-HR
M24	MPI-ESM-MR	M51	MPI-ESM1-2-LR
M25	MRI-CGCM3	M52	MRI-ESM2-0
M26	NorESM1-M	M53	NESM3
M27	NorESM1-ME	M54	NorCPM1
		M55	NorESM2-LM
		M56	UKESM1-0-LL

Table 1. The 27 CMIP5 and 29 CMIP6 models used in this study.

b. Methods

Interannual variability signals were extracted by removing the linear trend, the annual cycle, and a 13-year running mean from the original datasets. The boreal winter Niño-3.4 index is calculated as the December–January–February (D(0)JF(1)) SST anomalies averaged over 5°S–5°N, 120°–170°W. Here, the notation "(1)" refers to calendar months in the decaying year of El Niño, while "(0)" denotes the developing year.

Thermocline depth is defined as the depth of the 20°C isotherm (D20). The easterly wind (EW) index is used to quantify the climatological zonal wind averaged over the equatorial Indian Ocean (2°S–2°N, 70°E–90°E) during September–October–November (SON) in both observations and CMIP5/6 model simulations, with values multiplied by −1 to reflect the strength of easterly winds (Li et al. 2015). The cold tongue (CT) index is defined as the observed or simulated climatological SST averaged over the cold tongue region (2°S–2°N,

Accepted for publication in *Journal of Climate*. DOI 10.1175/JCLI-D-25-0438.1.

170°E–130°W) during DJF, minus the tropical Pacific mean SST (20°S–20°N, 0°–360°E), also multiplied by −1 to indicate cold tongue intensity (Jiang et al. 2020). DJF is chosen as it corresponds to the peak season of El Niño's influence on the Indian Ocean. The negative factor ensures that larger values of the EW and CT indices represent stronger easterly winds in the tropical Indian Ocean and colder SSTs in the Pacific cold tongue region, respectively.

The statistical significance of the correlation coefficients is evaluated using a two-tailed Student's t-test. Intermodel consensus is defined as the percentage of models that share the same sign of change as the multi-model ensemble mean (MME). A previous study suggested that a 68% consensus is considered statistically robust, corresponding to the 95% confidence level under the assumption of model independence (Power et al. 2012).

3. Biases and leading modes of intermodel spread in IOBM simulations in CMIP5 and CMIP6

The observed IOBM pattern during the decaying summer of ENSO is shown in Fig. 1a, obtained by regressing June–July–August [JJA(1)] Indian Ocean SST anomalies onto the unstandardized preceding winter (D(0)JF(1)) Niño-3.4 index over the period 1979–2005. The resulting pattern features basin-wide warming across the tropical Indian Ocean. Notably, stronger warm SST anomalies emerge in the subtropical southwestern, northwestern, and eastern Indian Ocean (EIO), while weak cold anomalies appear in the equatorial western Indian Ocean (WIO). However, both the CMIP5 and CMIP6 MMEs exhibit systematic biases in reproducing the IOBM (Figs. 1b–c). Specifically, SST anomalies in the subtropical southwestern, northwestern, and EIO are cooler than observed, whereas the WIO displays a warm bias. These regions are also characterized by large intermodel spread, highlighting substantial discrepancies among models (Figs. 1b–c).

To further evaluate model performance, we quantify SST anomaly biases over the WIO (10°S–10°N, 40°–60°E) and EIO (green trapezoid in Fig. 1b) for both the CMIP5 and CMIP6 MMEs as well as for individual models (Figs. 1d–e). Although bias magnitudes vary across models, most simulate a warm bias in the WIO and a cold bias in the EIO. Only a few models reproduce relatively realistic SST anomalies—defined here as bias magnitudes smaller than 0.01—in these regions. For the WIO (Fig. 1d), this includes 2 CMIP5 models (ACCESS1-0, CSIRO-Mk3-6-0) and 2 CMIP6 models (CanESM5 and CNRM-CM6-1). For the EIO (Fig. 1e), only 3 CMIP6 models (EC-Earth3, FGOALS-f3-L, and MIROC-ES2L) meet this criterion. These results indicate that simulating the EIO portion of the IOBM pattern poses a greater

Accepted for publication in *Journal of Climate*. DOI 10.1175/JCLI-D-25-0438.1.

challenge than the WIO, as also reflected in the larger MME biases in the EIO region in both CMIP5 and CMIP6 (Figs. 1d–e). While CMIP6 models exhibit slightly smaller MME biases than CMIP5 models in both regions, both generations display a substantial intermodel spread. This suggests that, despite modest improvements in ensemble mean performance, no significant progress has been made in accurately simulating the IOBM structure during ENSO decay summers between CMIP5 and CMIP6.

Accepted for publication in *Journal of Climate*. DOI 10.1175/JCLI-D-25-0438.1.

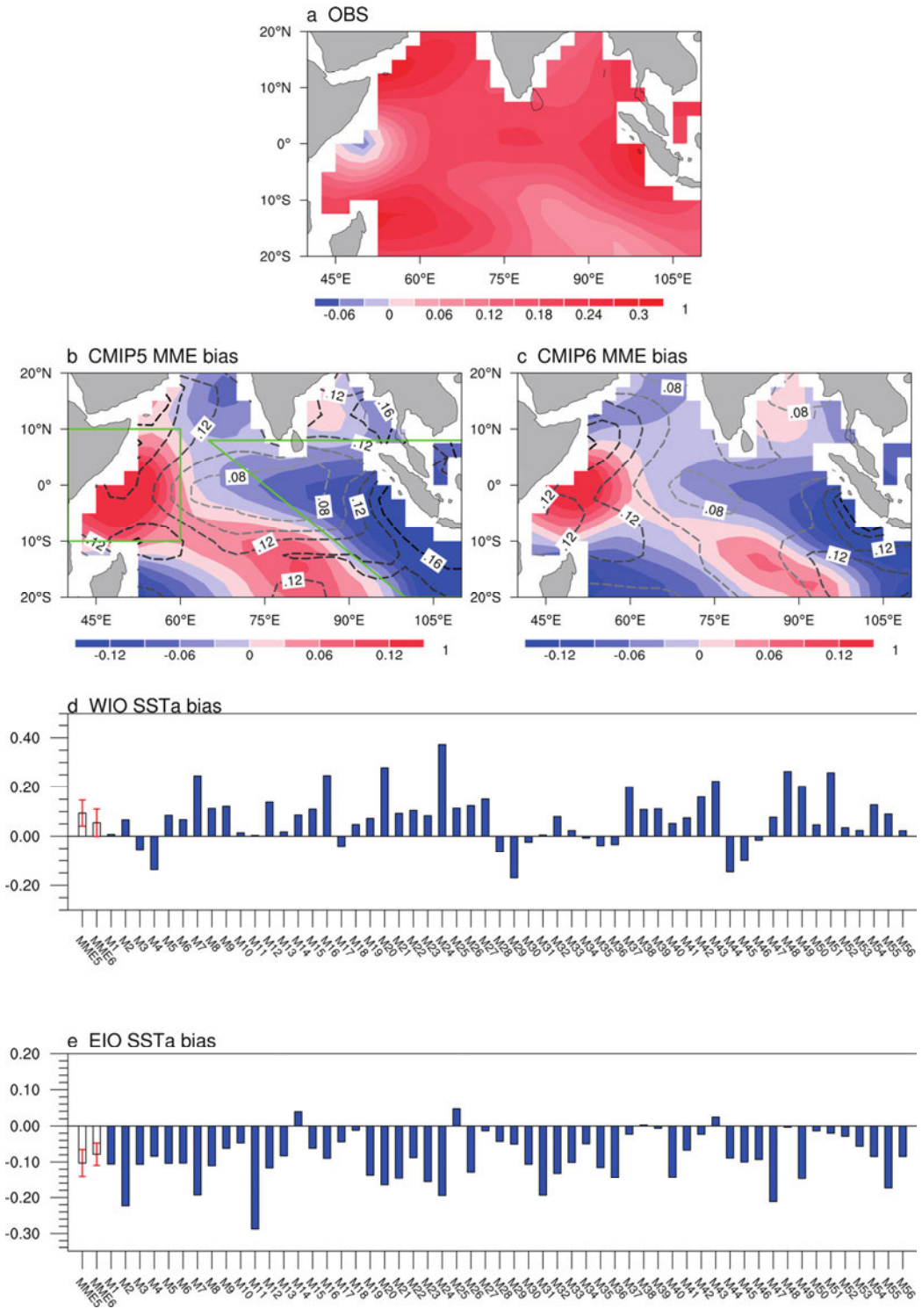

Fig. 1. IOBM patterns during ENSO decay summers [JJA(1)] in (a) observations, and associated model biases in (b) the CMIP5 multi-model ensemble (MME) and (c) the CMIP6 MME. Shading in panels (a)–(c) represents SST anomalies regressed onto the D(0)JF(1) Niño-3.4 index, and contours in (b) and (c) indicate intermodel standard deviations. The green box and trapezoid mark the WIO and EIO regions used for area-mean calculations, respectively. Panels (d) and (e) show the corresponding area-mean ENSO-related SST anomaly biases in the WIO and EIO for the CMIP5 and CMIP6 MMEs, respectively, along with results from individual models.

Accepted for publication in *Journal of Climate*. DOI 10.1175/JCLI-D-25-0438.1.

To investigate the sources of model bias in simulating the IOBM in CMIP5 and CMIP6, we first examine the leading patterns of intermodel spread in IOBM simulations by using an intermodel EOF analysis. This approach highlights models diverge in simulating the IOBM response to ENSO forcing and serves as an effective diagnostic to identify structural biases commonly shared among models and to infer underlying causes of IOBM simulation biases, which has been widely employed to extract leading patterns of model biases in CMIP models (Zhou et al. 2020, 2019; Jiang et al. 2021, 2022; Liu et al. 2023).

We perform an intermodel EOF analysis on regression coefficient maps of JJA(1) Indian Ocean SST anomalies onto the preceding winter (D(0)JF(1)) Niño-3.4 index. These maps are derived from 56 CMIP5 and CMIP6 models, as detailed in Figure 1, and cover the tropical Indian Ocean domain (20°S–20°N, 35°–115°E). The first EOF mode accounts for 28.28% of the total variance in the intermodel spread and features a dipole-like pattern reminiscent of the Indian Ocean Dipole (IOD), with negative SST anomalies centered in the WIO and positive anomalies in the EIO (Fig. 2a). This indicates that IOD-like variability is a dominant contributor to the intermodel spread in simulated IOBM. The second EOF mode explains 20.09% of the variance and exhibits a monopole structure, characterized by negative SST anomalies centered in the EIO (Fig. 2b). This mode reflects an additional and independent source of model disagreement, distinct from the IOD-like mode. The separation between these two EOF modes was evaluated using North's rule of thumb test (North et al., 1982), which confirms that they are statistically well separated and may be regarded as independent modes.

Accepted for publication in *Journal of Climate*. DOI 10.1175/JCLI-D-25-0438.1.

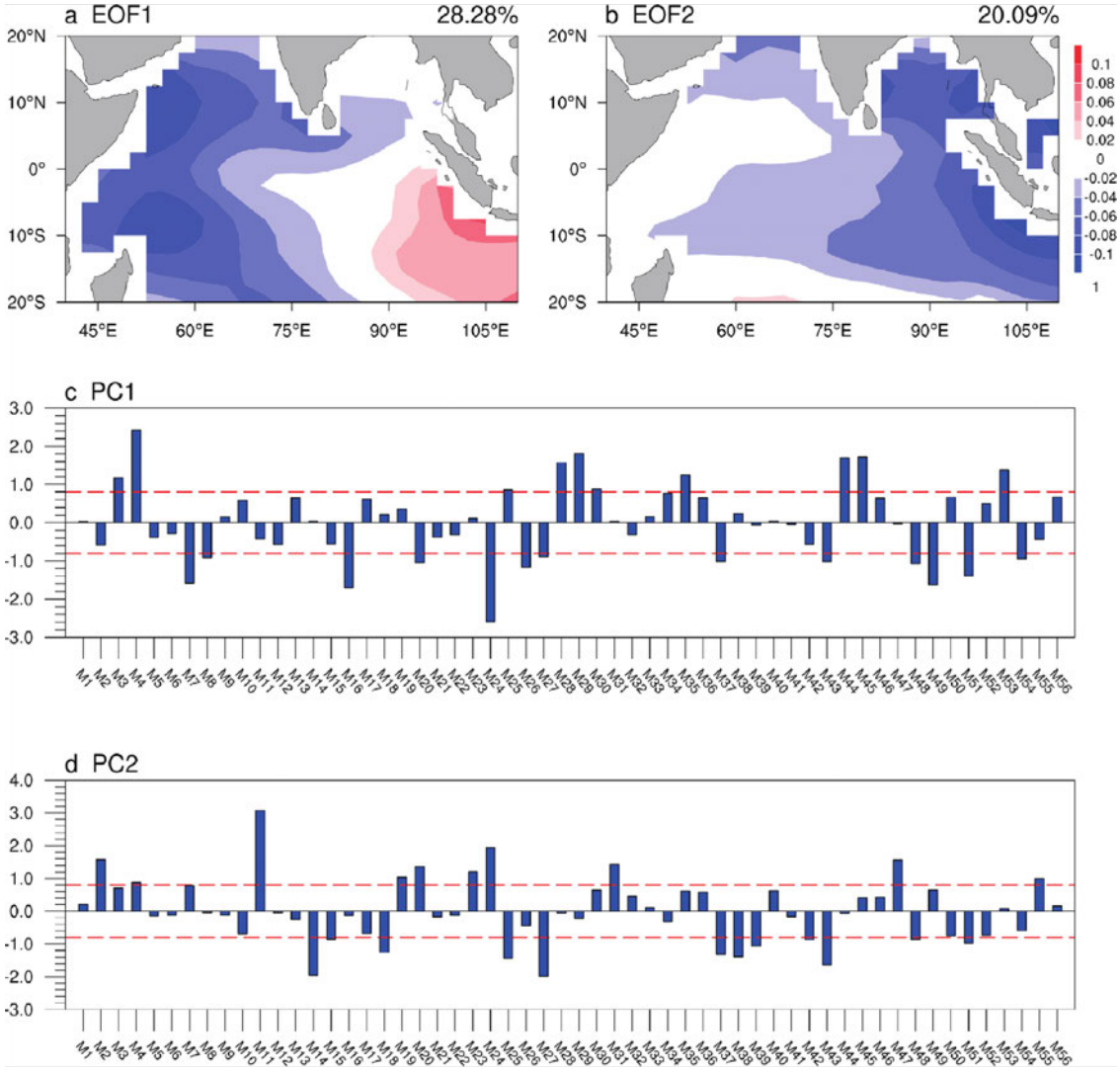

Fig. 2. (a) First and (b) second EOF modes of intermodel differences in the regression of JJA(1) Indian Ocean SST anomalies onto the preceding winter (D(0)JF(1)) Niño-3.4 index, based on 56 CMIP5 and CMIP6 models. The percentage values at the top-right in panels (a) and (b) indicate the fraction of total intermodel variance explained by each mode. These two EOF modes are statistically well separated according to North's rule of thumb test (North et al., 1982). Panels (c) and (d) display the corresponding principal component scores (PC1 and PC2) for each model. Red dashed lines in panels (c) and (d) indicate ±0.8 standard deviations, used as thresholds for model grouping in subsequent analyses.

4. Origins and Mechanisms of Intermodel Spread in IOBM Biases

As discussed earlier, previous studies have suggested that biases in simulating the IOBM are influenced by how models represent the climatological easterly winds over the equatorial Indian Ocean and the cold tongue in the equatorial Pacific (Du et al. 2013; Jiang et al. 2017, 2021; Li et al. 2015; Tao et al. 2016; Weller and Cai 2013; Zheng et al. 2016). It is plausible that the two leading EOF modes of intermodel spread in IOBM simulations reflect the distinct

Accepted for publication in *Journal of Climate*. DOI 10.1175/JCLI-D-25-0438.1.

impacts of these mean-state biases in the Indian and Pacific Oceans. To explore these potential connections, we examine the relationships between the principal components of the first two EOF modes (PC1 and PC2; Figs. 2c–d) and the EW and CT indices across the 56 CMIP5/6 models. PC1 exhibits a significant positive correlation with the EW index ($r = 0.39$, $p<0.01$; Fig. 3a), but a weaker and statistically insignificant correlation with the CT index ($r = 0.21$, $p > 0.1$; Fig. 3b). Conversely, PC2 shows a strong and significant correlation with the CT index ($r = 0.56$, $p < 0.01$; Fig. 3c), while its correlation with the EW index is weak and negative ($r = -0.21$, $p > 0.1$; Fig. 3d). These results suggest that the first EOF mode is primarily associated with variations in the strength of climatological easterly winds over the Indian Ocean, whereas the second EOF mode is more strongly linked to differences in the intensity of the Pacific cold tongue. Given the potential concern that the EW and CT indices may not be fully independent, we examined their relationship across the CMIP5/6 models. The two indices show only a weak and statistically insignificant correlation ($r = 0.22$, $p > 0.1$; figure not shown), indicating that they are largely independent and can be regarded as distinct sources of intermodel spread in IOBM simulations. In addition, although the correlation between PC1 and the EW index is moderate, it is statistically significant ($p < 0.01$), suggesting that zonal SST gradient biases and associated equatorial Indian Ocean winds are a key driver of EOF1, while acknowledging that other processes may also contribute.

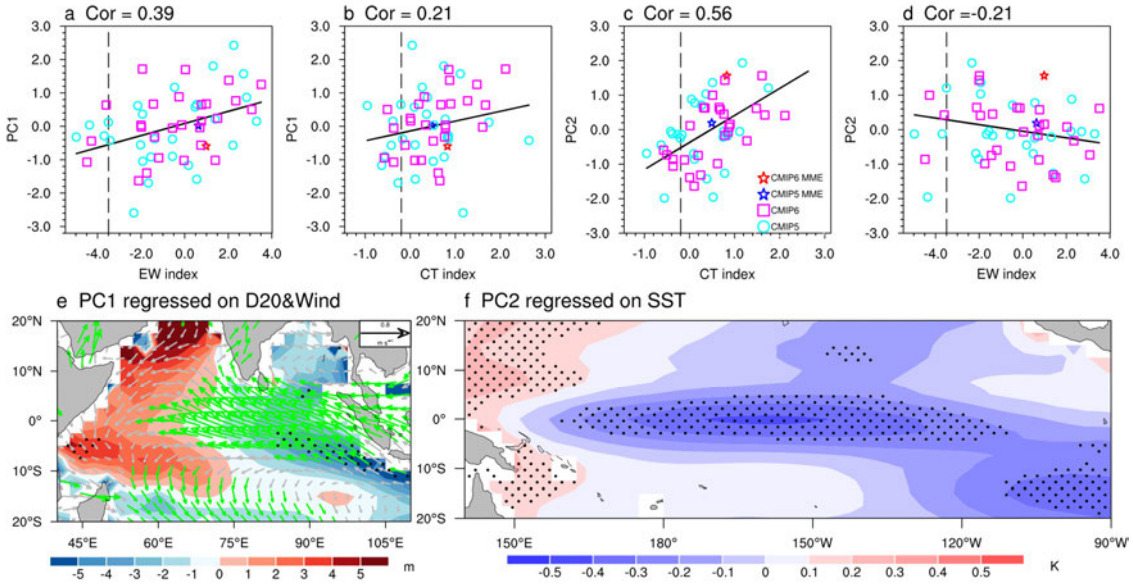

Fig. 3. Intermodel relationships between (a) PC1 and the EW index, and (b) PC1 and the CT index. Panels (c) and (d) show intermodel correlations between PC2 and the CT index, and PC2 and the EW index, respectively. Linear correlation coefficients are shown in the top-left corner of each panel, with solid black lines indicating the linear regression fits. Dashed lines along the horizontal axes represent the observed present-day values of the EW index (in panels a and d) and the CT index (in panels b and c), both multiplied

Accepted for publication in *Journal of Climate*. DOI 10.1175/JCLI-D-25-0438.1.

by −1. (e) Intermodel regression of climatological SON 925-hPa winds and DJF thermocline depth (D20) over the Indian Ocean onto standardized PC1 across 56 CMIP5 and CMIP6 models. (f) Intermodel regression of DJF climatological SST over the Pacific onto standardized PC2. Stippling in panels (e) and (f), and green wind vectors in (e), indicate regions where the regression is statistically significant at the 90% confidence level based on a Student's t-test.

To further examine these associations and to highlight the key regions where each mode aligns with documented mean-state biases—namely, the Indian Ocean fields for PC1 and the Pacific fields for PC2—we regress PC1 and PC2 onto climatological SON surface winds and DJF thermocline depth over the Indian Ocean, as well as DJF climatological SST over the Pacific Ocean, across the 56 CMIP5/6 models. These regressions reveal the mean-state bias patterns linked to each intermodel EOF mode. We use DJF climatology for thermocline depth to account for the lagged oceanic adjustment to wind forcing. The first EOF mode, which exhibits an IOD-like dipole structure, is closely linked to the strength of easterly winds over the equatorial Indian Ocean (Fig. 3e). Models with stronger climatological easterlies during SON tend to produce a west–east slope in the climatological thermocline during DJF, with the thermocline (D20) shoaling toward the eastern Indian Ocean (EIO). The second EOF mode, marked by a monopole pattern with negative SST anomalies centered over the EIO, is strongly associated with the cold tongue bias in the equatorial Pacific (Fig. 3f).

In addition, Figs. 3a–d show that CMIP6 models exhibit no substantial improvement over CMIP5 in representing either the climatological easterly winds over the equatorial Indian Ocean or the Pacific cold tongue. The distributions of both the EW and CT indices remain broadly similar between the two model generations, as seen in the MME values from CMIP5 and CMIP6, suggesting that these persistent mean-state biases continue to limit the accurate simulation of the IOBM.

a. Influence of climatological equatorial easterly wind bias on IOBM simulation

To investigate how climatological easterly winds over the Indian Ocean influence the EOF1 mode of intermodel spread in IOBM simulations, we contrast two groups of CMIP5/6 models: 10 models with strongly positive PC1 values (PC1 > 0.8; Group A) and 13 models with strongly negative PC1 values (PC1 < –0.8; Group B). These groups represent opposing phases of the EOF1 mode, enabling a comparison of their climatological states and associated IOBM responses.

Consistent with the regression patterns shown in Fig. 3e, both groups exhibit easterly wind biases over the equatorial Indian Ocean during SON (Figs. 4d–e). These enhanced easterlies

Accepted for publication in *Journal of Climate*. DOI 10.1175/JCLI-D-25-0438.1.

induce a west–east tilt in the climatological thermocline during DJF, intensify upwelling in the EIO, and drive westward advection of surface waters. This leads to a deepening of the thermocline in the southwestern and northwestern Indian Ocean via Ekman convergence (Figs. 4d–e). Compared with observed thermocline climatology (Fig. 4c), both groups show a positive depth bias in the WIO and a negative bias in the EIO (Figs. 4a, b, d, e). However, Group A features a stronger easterly wind bias, resulting in a more pronounced thermocline tilt, with depths exceeding observed values by over 20 meters (Fig. 4d). In contrast, Group B exhibits smaller biases, generally under 10 meters, and more closely aligned with observations (Fig. 4e). The climatological differences between the two groups in wind and thermocline structure closely resemble the PC1-regressed patterns (Figs. 4f, 3e).

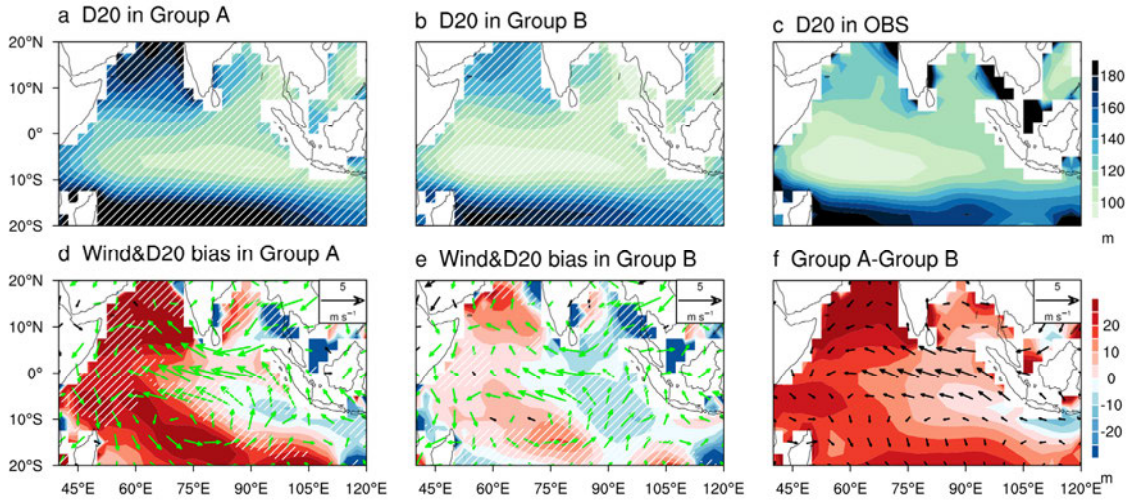

Fig. 4. Climatological thermocline depth in winter (DJF) (shadings, m) for (a) Group A, (b) Group B and (c) observations, and MME biases in climatological surface wind (vectors, m s–1) in autumn (SON) and thermocline depth in winter (DJF) for (d) Group A, (e) Group B, and (f) the MME difference between Group A and Group B. Stippled regions and green vectors in (a)–(b) and (d)–(e) indicate where the sign of the MME agrees in more than 68% of models. The MME difference in (f) represents a contrast between ensemble means rather than a statistically tested difference.

The background thermocline depth plays a critical role in modulating the strength of thermocline–SST coupling on interannual timescales. SST anomalies are more sensitive to vertical thermocline variations when the mean thermocline is shallower. Although thermocline anomalies in the southwestern Indian Ocean during the El Niño mature winter [D(0)JF(1)] are of similar magnitude in both groups (Figs. 5a, d), the deeper background thermocline in Group A suppresses the SST response (Fig. 5g). Consequently, SST anomalies in the southwestern Indian Ocean remain weak into the following spring [MAM(1)], resulting in weaker cross-equatorial antisymmetric wind anomalies (Figs. 5b, e, h) and a reduced IOBM amplitude during

Accepted for publication in *Journal of Climate*. DOI 10.1175/JCLI-D-25-0438.1.

the El Niño decay summer [JJA(1)] relative to observations (Figs. 5c, 1a). These results are consistent with previous studies (Li et al. 2015; Zheng et al. 2016).

In contrast, Group B's smaller thermocline depth biases in the southwestern Indian Ocean (Figs. 4b, e) enable stronger thermocline–SST coupling, which facilitates the development of warm SST anomalies in the WIO and associated antisymmetric wind anomalies during MAM(1) (Fig. 5e). This, in turn, promotes a second warming in the northern Indian Ocean during JJA(1) (Fig. 5f), consistent with the mechanism described by Du et al. (2009). However, Group B also shows a systematic bias of strong easterlies and a shallower-than-observed thermocline in the EIO (Fig. 4e). As a result, when easterly anomalies occur over the EIO, enhanced upwelling of cold subsurface water cools the SST anomalies in the EIO and favors the development of a positive IOD-like pattern (Figs. 5d–f), consistent with previous studies (Cai et al. 2011; Cai and Cowan 2013; McKenna et al. 2024; Weller and Cai 2013). The pattern of bias differences between Groups A and B closely resembles the EOF1 structure (Figs. 5i, 2a).

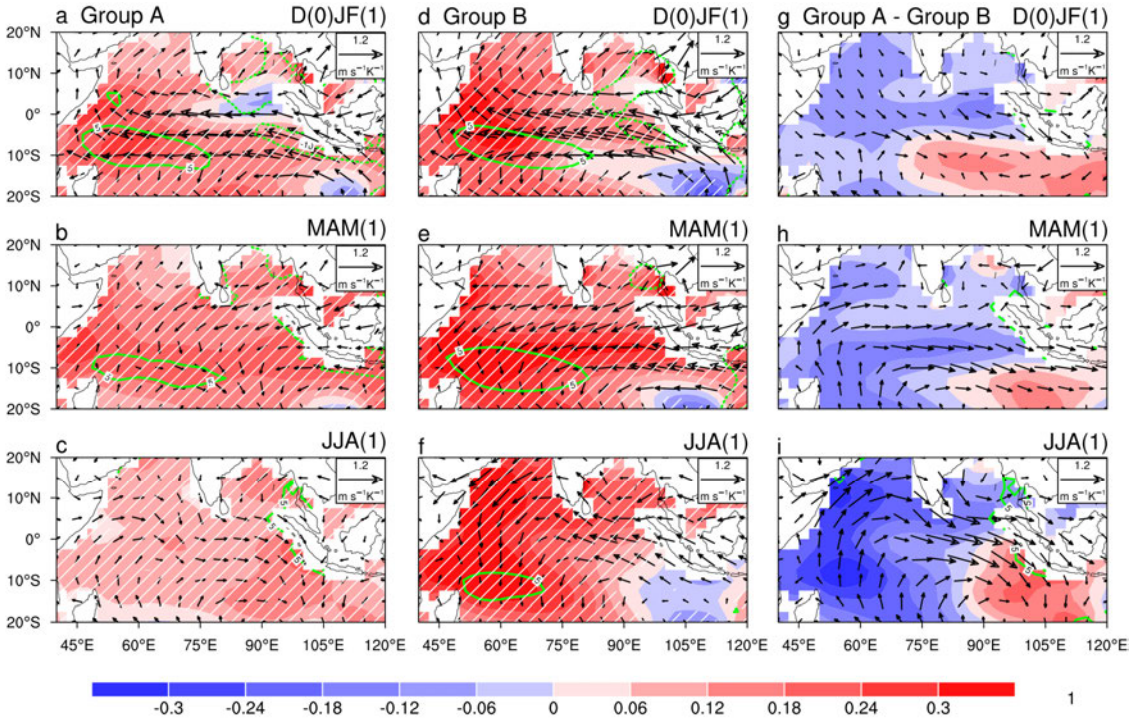

Fig. 5. ENSO-related anomalies for (a–c) Group A, (d–f) Group B, and (g–i) the MME difference between the two groups. Anomalies of SST (shading, non-dimensional), thermocline depth (contours, m K^{-1}) and 925-hPa winds (vectors, m s^{-1} K^{-1}) from D(0)JF(1) to JJA(1). Stippled regions in (a)-(f) indicate where the sign of the MME agrees in more than 68% of models. The MME difference in (g)-(i) represents a contrast between ensemble means rather than a statistically tested difference.

Accepted for publication in *Journal of Climate*. DOI 10.1175/JCLI-D-25-0438.1.

These results highlight that the impact of climatological easterly wind bias on the simulated IOBM depends critically on its intensity. When the easterly bias is strong and accompanied by an excessively deep background thermocline in the southwestern Indian Ocean, the thermocline–SST coupling is weakened, leading to a suppressed IOBM amplitude, particularly over the southwestern and northwestern basin. By contrast, when the easterly bias is moderate, the thermocline in the southwest remains shallow enough to sustain strong thermocline–SST coupling, enabling the development of warm SST anomalies in the southwestern and northern Indian Ocean. At the same time, the easterly bias shoals the background thermocline in the eastern Indian Ocean, favoring cold SST anomalies and reinforcing a positive IOD-like structure. Taken together, these findings clarify why EOF1, despite its zonal SST dipole pattern, captures the intermodel spread of IOBM amplitude and provide new insight into how mean-state easterly wind biases shape the diversity of IOBM simulations across climate models.

b. Influence of climatological cold tongue bias on IOBM simulation

Using a similar approach, we examine the influence of biases in the Pacific cold tongue climatology on IOBM simulations. Based on standardized PC2 values, we select ten models with PC2 > 0.8 as Group C and twelve models with PC2 < –0.8 as Group D. Compared to observations, both groups simulate an overly westward-extended DJF climatological cold tongue in the equatorial Pacific (Figs. 6a–e), with the bias more pronounced in Group C (Fig. 6f).

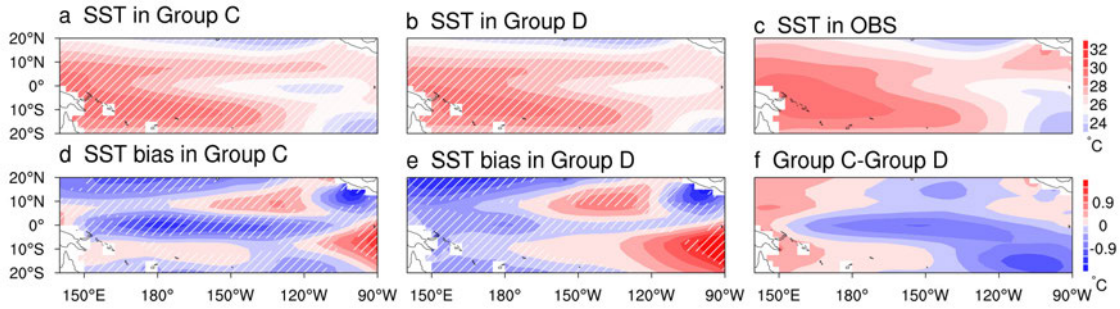

Fig. 6. Climatological SST (shading, °C) during winter (DJF) for (a) Group C, (b) Group D, and (c) observations, and MME biases of climatological SST for (d) Group C, (e) Group D, and (f) the difference between the two groups. Stippled regions in (a)-(b) and (d)-(e) indicate where the sign of the MME agrees in more than 68% of models. The MME difference in (f) represents a contrast between ensemble means rather than a statistically tested difference.

Previous studies have shown that an excessively westward-extended cold tongue can lead to simulated ENSO-related SST anomalies that also extend too far west and decay more slowly

Accepted for publication in *Journal of Climate*. DOI 10.1175/JCLI-D-25-0438.1.

than observed. This is due to an overly strong zonal advection feedback, involving ENSO-induced current anomalies and the climatological SST gradient associated with the cold tongue (Jiang et al. 2017, 2021). Relative to observations (Figs. 7a–c), Group C simulates ENSO events that extend approximately 20° farther west during the peak DJF season, with anomalous warm SSTs persisting from D(0)JF(1) through JJA(1) (Figs. 7d–f). Group D also exhibits westward extension and delayed decay, but with weaker intensity (Figs. 7g–i).

As emphasized earlier, both EOF1 and EOF2 ultimately affect the IOBM through the same physical mechanism: ENSO-induced interannual easterly anomalies over the equatorial Indian Ocean excite downwelling Rossby waves that propagate into the southwestern Indian Ocean, where they modulate the thermocline, trigger local SST warming, and induce antisymmetric cross-equatorial winds that counteract the boreal summer monsoon. However, the two modes differ in their entry points into this shared pathway.

In Group C, the lingering warm SST anomalies in the western Pacific influence IOBM development and the simulation of the capacitor effect through two key pathways. First, the westward-extended Pacific anomalies enhance the Walker circulation, which reduces ENSO-induced interannual easterly anomalies over the equatorial Indian Ocean during D(0)JF(1) (Figs. 7a, d, g, j). This weakens downwelling Rossby waves, the associated SST response in the southwestern Indian Ocean, and subsequent antisymmetric wind anomalies during MAM(1) (Xie et al. 2002; Masumoto and Meyers 1998) (Figs. 7b, e, h, k). Second, the westward-shifted convection anomalies induce a Gill-type atmospheric response, generating off-equatorial cyclonic anomalies that extend into the eastern Indian Ocean during JJA(1). The southern cyclone strengthens local climatological winds, enhances evaporative cooling (highlighted by magenta contours in Fig. 7f), and drives cold SST anomalies, while the northern cyclone over the South China Sea weakens and shifts eastward the Northwest Pacific anticyclone (Fig. 7f), disrupting Indo–western Pacific feedback and further dampening northern Indian Ocean warming. Together, these processes weaken the IOBM and the Indian Ocean capacitor effect (Xie et al. 2016).

In contrast, Group D—with weaker cold tongue biases and more realistic SST anomalies in the equatorial western Pacific—better reproduces the observed IOBM evolution and associated capacitor effect (Figs. 7i, c). The differences between the two groups closely resemble the second EOF mode of intermodel spread in IOBM simulations (Figs. 7l, 2b).

Accepted for publication in *Journal of Climate*. DOI 10.1175/JCLI-D-25-0438.1.

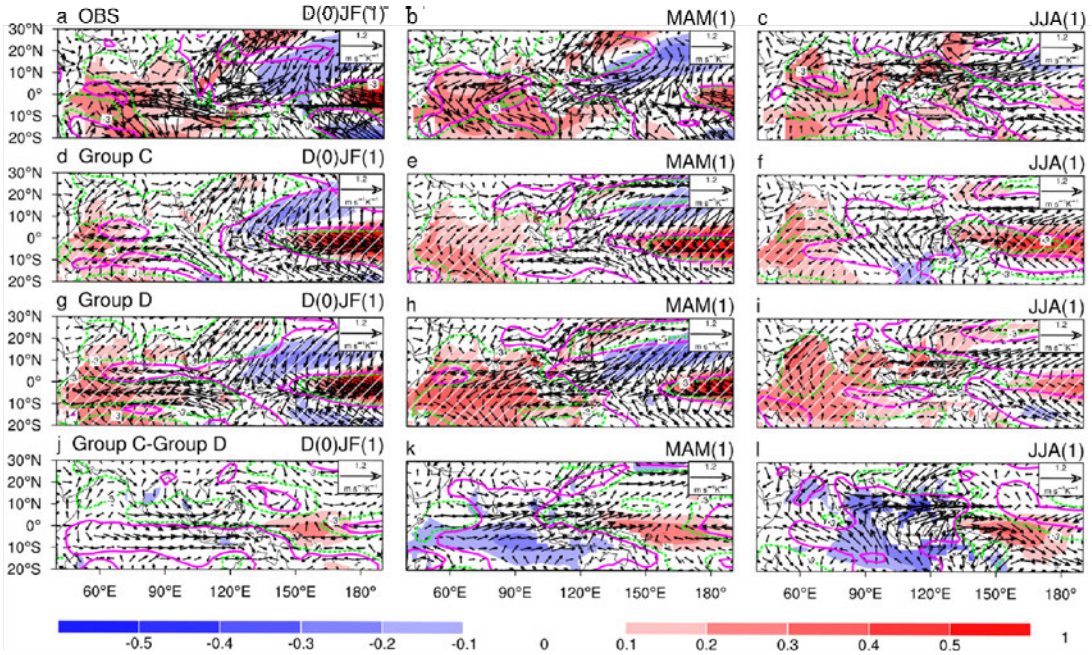

Fig. 7. ENSO-related anomalies in (a–c) observations, (d–f) Group C, (g–i) Group D, and (j–l) the MME difference between Groups C and D. Shading shows SST anomalies (°C), contours represent latent heat flux anomalies (W m^{-2} K^{-1}; positive upward, with magenta lines for +3 and green lines for –3), and vectors indicate 925-hPa wind anomalies (m s^{-1} K^{-1}) from D(0)JF(1) to JJA(1). Stippling marks regions where more than 68% of models in the MME agree on the sign of the anomaly. The MME difference in (j–l) represents a contrast between ensemble means rather than a statistically tested difference.

Overall, EOF2 primarily reflects the remote influence of the Pacific cold-tongue bias on the ENSO–IOBM linkage. Through its control on the Walker circulation and the westward extent of ENSO convection, the cold tongue bias alters both the strength of ENSO-induced interannual easterlies over the Indian Ocean and the Gill-type atmospheric response over the EIO. The combined effects of these atmospheric pathways lead to a distinct EIO-centered SST bias pattern captured by EOF2, in contrast to the mean-state-driven processes represented by EOF1. While the Indonesian Throughflow may modulate Pacific–Indian Ocean exchanges, its role is likely secondary given the coarse resolution of ITF passages in most CMIP models and is not investigated in this study.

5. Implications for projections of the IOBM and its capacitor effect

The results above demonstrate that biases in the climatological easterly winds over the equatorial Indian Ocean and in the climatological cold tongue in the equatorial Pacific significantly influence the simulations of the IOBM and its capacitor effect in CMIP5 and CMIP6 models. To further investigate how these biases may affect future projections of the IOBM and its associated capacitor effect, we examine the relationships between model

Accepted for publication in *Journal of Climate*. DOI 10.1175/JCLI-D-25-0438.1.

climatological biases in historical simulations and projected changes in IOBM-related variables. Historical simulations cover the period 1979–2005, while future projections span 2070–2096 under the RCP8.5 (CMIP5) and SSP5-8.5 (CMIP6) scenarios. To reduce the influence of intermodel spread in global mean warming, all projected changes are normalized by each model's SST increase averaged over 60°S–60°N.

To quantify the strength of the Indian Ocean capacitor effect, we follow previous studies (Hu et al. 2014, 2021; Tao et al. 2015; Xie et al. 2009) and use tropical tropospheric temperature (TT) anomalies over the Indian Ocean. TT anomalies are a key component of the capacitor effect mechanism, which enables the IOBM to sustain ENSO's influence beyond the peak of El Niño. Once the IOBM is established in JJA(1), associated Indian Ocean warming can trigger a Gill-type atmospheric response, including an eastward-propagating Kelvin wave that spreads TT anomalies into the western Pacific. This process affects regional climate phenomena such as the western Pacific summer high and monsoon systems (Chen et al. 2019; Xie et al. 2009; Yang et al. 2007; Jiang et al. 2019, 2018; Huang et al. 2010). Therefore, JJA(1) TT anomalies over the Indian Ocean provide an effective measure of the strength of the Indian Ocean capacitor effect.

Our analysis reveals an overall negative relationship between the magnitude of model climatological biases and El Niño–induced TT anomalies over the Indian Ocean. Specifically, the projected changes in JJA(1) TT anomalies under warming scenarios exhibit significant negative regressions against the climatological biases in (i) SON easterly wind strength over the equatorial Indian Ocean and (ii) DJF cold tongue strength in the Pacific (Figs. 8a–b). The correlation between the SON easterly wind bias and TT changes reaches –0.36, and that between the DJF cold tongue bias and TT change is –0.43—both significant at the 99% confidence level (Figs. 8a–b). These results indicate that stronger climatological mean-state biases suppress the projected enhancement of the Indian Ocean capacitor effect.

Accepted for publication in *Journal of Climate*. DOI 10.1175/JCLI-D-25-0438.1.

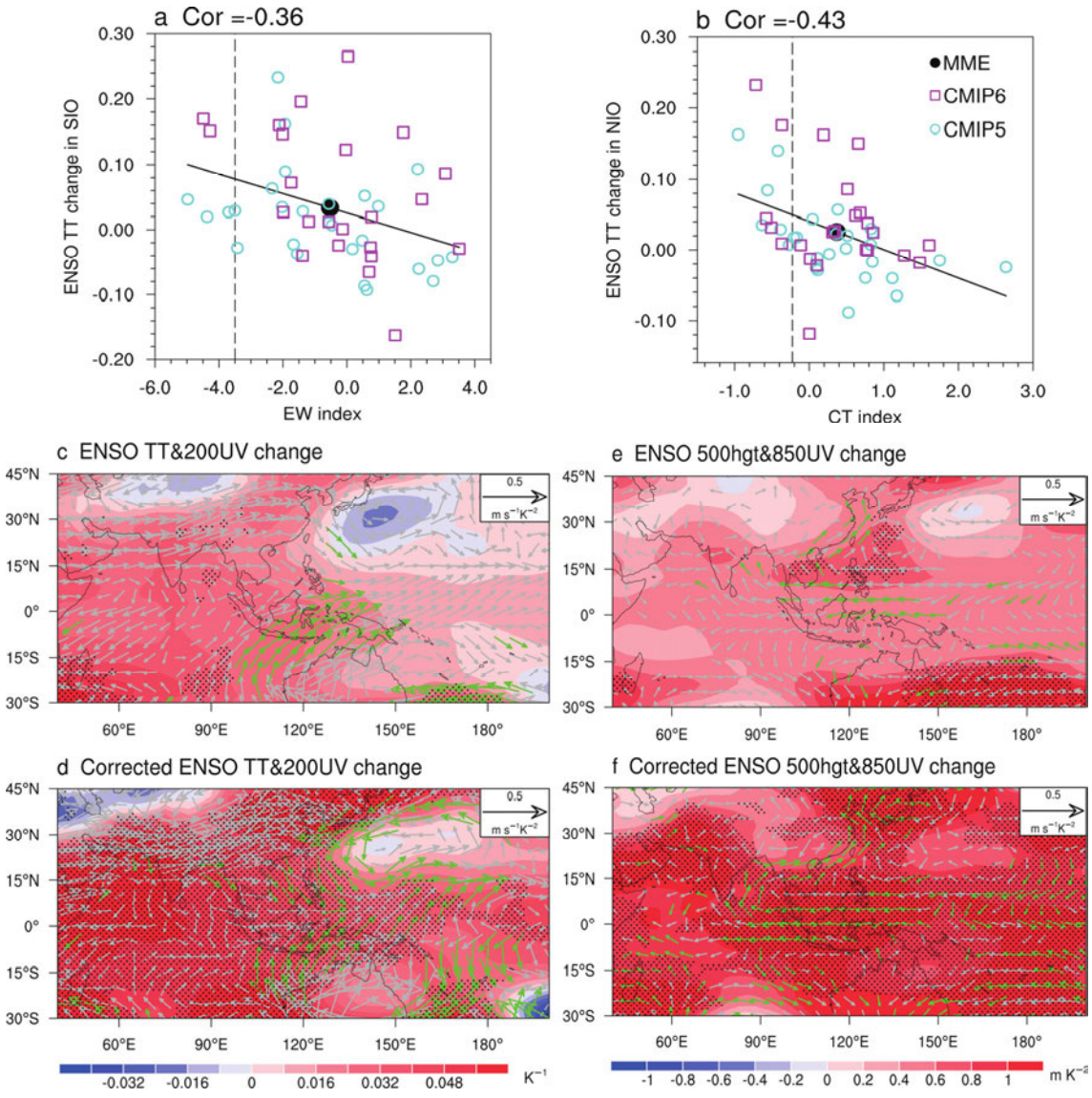

Fig. 8. (a) Scatterplots of the SON easterly wind (EW) index versus projected changes in Nino3.4-regressed tropospheric temperature anomalies over the south Indian Ocean during JJA(1). (b) Scatterplots of the DJF cold tongue (CT) index versus projected changes in Nino3.4-regressed tropospheric temperature over the northern Indian Ocean in 56 models. The intermodel correlation coefficients of the 56 models are shown in the top-left of the panels. All correlation coefficients are significant at the 99% confidence level, based on the Student's t-test. (c) MME changes in ENSO-related tropospheric temperature (925-200hPa mean) and 200-hPa wind anomalies in the period 2070-2096 relative to those in 1979-2005. (d) Observational constraint on changes in ENSO-related tropospheric temperature and 200-hPa wind anomalies. (e) MME changes in ENSO-related 500-hPa geopotential height and 850-hPa wind anomalies and (f) their observationally constrainted counterparts.

Consistent with previous studies (Hu et al. 2014; Zheng et al. 2011), we find that the Indian Ocean capacitor effect tends to strengthen under greenhouse warming. This is shown in Figure 8b, where the MME of CMIP5/6 models exhibits intensified El Niño–induced TT anomalies

Accepted for publication in *Journal of Climate*. DOI 10.1175/JCLI-D-25-0438.1.

over the Indian Ocean in the future climate compared to the historical period. However, this raw projection does not account for the influence of model biases in Indo-Pacific climatology. To refine this projection, we perform an observational constraint by the observed easterly wind strength and cold tongue strength based on the relationships derived in Figures 8a–b, following the approach of previous studies (Cox et al. 2013, 2018; Jiang et al. 2020; Li et al. 2017; Huang and Ying 2015; Zhou et al. 2019).

To correct for equatorial Indian Ocean easterly wind bias, we multiply the MME EW index bias (model-simulated minus observed) by the intermodel regression coefficient of TT change onto the EW index, yielding a grid-level correction that is subtracted from the original TT projection (Fig. 8c). A similar procedure is applied using the CT index to correct for Pacific cold tongue bias. The resulting bias-corrected projection is shown in Figure 8d, which reveals a more robust strengthening of the capacitor effect and improved intermodel consistency relative to the uncorrected projection in Figure 8c. In addition, similar analyses reveal enhanced 500-hPa geopotential height and 850-hPa anticyclonic anomalies over the northwestern Pacific (Figs. 8d, f), indicating a stronger northwestern Pacific anticyclone anomalies (NWPAC) response consistent with an intensified Indian Ocean capacitor effect.

These findings suggest that both easterly wind and cold tongue biases act to suppress the projected intensification of the Indian Ocean capacitor effect under global warming. After accounting for model climatological biases, the refined projection indicates that the future strengthening of the capacitor effect—and the associated NWPAC response—may be greater than previously estimated. Analyses of medium-emission scenarios (RCP4.5 and SSP2-4.5) similarly show a strengthened capacitor effect, with an even greater enhancement after observational constraint (figure not shown), confirming the robustness of our conclusions. Importantly, this pilot analysis demonstrates the value of incorporating mean-state bias diagnostics into future projection assessments. While more comprehensive analyses are needed, our results highlight the potential of this approach to improve the reliability of Indian Ocean capacitor effect projections.

6. Conclusions and Discussions

This study systematically assesses the simulation of the IOBM using outputs from 56 CMIP5 and CMIP6 models. We identify two dominant modes of intermodel spread in IOBM simulations: (1) an IOD-like mode associated with biases in the climatological easterly winds over the equatorial Indian Ocean, and (2) an EIO-centered mode linked to biases in the

Accepted for publication in *Journal of Climate*. DOI 10.1175/JCLI-D-25-0438.1.

climatological cold tongue in the equatorial Pacific. Moreover, local Indian Ocean easterly wind biases impact IOBM simulation more than Pacific cold tongue biases. Comparing CMIP5 and CMIP6 model performance, we find no substantial improvement in IOBM simulation in CMIP6.

Our analysis shows that models with stronger easterly wind biases tend to deepen the thermocline in the southwestern Indian Ocean, weakening SST–thermocline coupling and suppressing the IOBM amplitude. In contrast, models with weaker easterly wind biases favor stronger Bjerknes feedback, shifting the IOBM toward an IOD-like spatial pattern. Similarly, models with stronger cold tongue biases exhibit westward-extending ENSO SST anomalies and reduced cross-basin air-sea interactions, both of which diminish the IOBM amplitude, especially in EIO.

Critically, these climatological biases in easterly winds and cold tongue structure also suppress the strength and intermodel agreement of projected El Niño–related TT anomalies over the Indian Ocean—key indicators of the Indian Ocean capacitor effect. When projections are constrained by observed mean-state conditions, the projected TT anomalies become stronger and more consistent across models, suggesting that current models may underestimate the future enhancement of the Indian Ocean capacitor effect under global warming. These results highlight the importance of mean-state biases—particularly in tropical surface winds, SST, and thermocline depth—in shaping both historical IOBM behavior and future projections.

The origin of the Indian Ocean easterly wind bias likely involves both atmospheric and coupled feedback processes. Long et al. (2020) demonstrated that this bias primarily arises from two sources: (1) an overly strong South Asian summer monsoon, which advects excessive easterly momentum toward the equator and triggers a convection–circulation feedback, and (2) coupling-induced warm SST biases in the western Indian Ocean that amplify the easterlies through the Bjerknes feedback. Together, these processes modify the zonal thermocline slope and can help explain the persistent easterly wind bias identified in this study.

Future research should further investigate the physical mechanisms by which easterly wind and cold tongue biases modulate the projections of the Indian Ocean capacitor effect, and explore their broader implications for ENSO variability and monsoon systems in a warming climate. Addressing these persistent model deficiencies will be critical for improving regional climate projections and understanding Indo-Pacific climate interactions.

Acknowledgments.

Accepted for publication in *Journal of Climate*. DOI 10.1175/JCLI-D-25-0438.1.

This work was supported by the National Natural Science Foundation of China (NSFC; Grants 42476017, 42141019, 42425601 and 42005022) and the Guangdong Basic and Applied Basic Research Foundation (2023A1515012145).

Data Availability Statement.

The observed SST data used during this study is publicly available from the Extended Reconstructed SST, version 5 (ERSST. V5) dataset at https://psl.noaa.gov/data/gridded/data.noaa.ersst.v5.html. The NCEP reanalysis datasets are available from the NOAA/PSL at https://psl.noaa.gov/data/gridded/data.ncep.reanalysis.html. The SODA 2.2.4 data is available at https://apdrc.soest.hawaii.edu/datadoc/soda_2.2.4.php. The CMIP5 model datasets are available at https://esgf-node.llnl.gov/search/cmip5/. And the CMIP6 model datasets are publicly available at https://esgf-node.llnl.gov/search/cmip6/.

REFERENCES

Alexander, M. A., I. Blade, M. Newman, J. R. Lanzante, N. C. Lau, and J. D. Scott, 2002: The atmospheric bridge: the influence of ENSO teleconnections on air-sea interaction over the global oceans. *Journal of Climate*, **15**, 2205–2231, https://doi.org/10.1175/1520-0442(2002)015%253C2205:tabtio%253E2.0.co;2.

Cai, W., and T. Cowan, 2013: Why is the amplitude of the Indian Ocean Dipole overly large in CMIP3 and CMIP5 climate models? *Geophysical Research Letters*, **40**, 1200–1205, https://doi.org/10.1002/grl.50208.

Cai, W., A. Sullivan, T. Cowan, J. Ribbe, and G. Shi, 2011: Simulation of the Indian Ocean Dipole: A relevant criterion for selecting models for climate projections: IOD AND CLIMATE PROJECTIONS. *Geophys. Res. Lett.*, **38**, n/a-n/a, https://doi.org/10.1029/2010GL046242.

Carton, J. A., and B. S. Giese, 2008: A reanalysis of ocean climate using Simple Ocean Data Assimilation (SODA). *Monthly Weather Review*, **136**, 2999–3017, https://doi.org/10.1175/2007mwr1978.1.

Chakravorty, S., J. S. Chowdary, and C. Gnanaseelan, 2014: Epochal changes in the seasonal evolution of tropical Indian Ocean warming associated with El Niño. *Clim Dyn*, **42**, 805–822, https://doi.org/10.1007/s00382-013-1666-3.

Chen, M. Y., J. Y. Yu, X. Wang, and W. Jiang, 2019: The changing impact mechanisms of a diverse El Niño on the Western Pacific Subtropical High. *Geophysical Research Letters*, **46**, 953–962, https://doi.org/10.1029/2018GL081131.

Chowdary, J. S., and C. Gnanaseelan, 2007: Basin-wide warming of the Indian Ocean during El Niño and Indian Ocean dipole years. *Intl Journal of Climatology*, **27**, 1421–1438, https://doi.org/10.1002/joc.1482.

Accepted for publication in *Journal of Climate*. DOI 10.1175/JCLI-D-25-0438.1.

Cox, P. M., D. Pearson, B. B. Booth, P. Friedlingstein, C. Huntingford, C. D. Jones, and C. M. Luke, 2013: Sensitivity of tropical carbon to climate change constrained by carbon dioxide variability. *Nature*, **494**, 341–344, https://doi.org/10.1038/nature11882.

——, C. Huntingford, and M. S. Williamson, 2018: Emergent constraint on equilibrium climate sensitivity from global temperature variability. *Nature*, **553**, 319–322, https://doi.org/10.1038/nature25450.

Du, Y., S.-P. Xie, G. Huang, and K. Hu, 2009: Role of Air-Sea Interaction in the Long Persistence of El Niño-Induced North Indian Ocean Warming. *Journal of Climate*, **22**, 2023–2038, https://doi.org/10.1175/2008jcli2590.1.

——, ——, Y.-L. Yang, X.-T. Zheng, L. Liu, and G. Huang, 2013: Indian Ocean Variability in the CMIP5 Multimodel Ensemble: The Basin Mode. *Journal of Climate*, **26**, 7240–7266, https://doi.org/10.1175/JCLI-D-12-00678.1.

Eyring, V., S. Bony, G. A. Meehl, C. A. Senior, B. Stevens, R. J. Stouffer, and K. E. Taylor, 2016: Overview of the Coupled Model Intercomparison Project Phase 6 (CMIP6) experimental design and organization. *Geoscientific Model Development*, **9**, 1937–1958, https://doi.org/10.5194/gmd-9-1937-2016.

Hu, K., G. Huang, and R. Wu, 2013: A Strengthened Influence of ENSO on August High Temperature Extremes over the Southern Yangtze River Valley since the Late 1980s. *Journal of Climate*, **26**, 2205–2221, https://doi.org/10.1175/jcli-d-12-00277.1.

——, ——, X.-T. Zheng, S.-P. Xie, X. Qu, Y. Du, and L. Liu, 2014: Interdecadal Variations in ENSO Influences on Northwest Pacific-East Asian Early Summertime Climate Simulated in CMIP5 Models. *Journal of Climate*, **27**, 5982–5998, https://doi.org/10.1175/jcli-d-13-00268.1.

——, ——, P. Huang, Y. Kosaka, and S.-P. Xie, 2021: Intensification of El Nino-induced atmospheric anomalies under greenhouse warming. *Nature Geoscience*, https://doi.org/10.1038/s41561-021-00730-3.

Huang, B., and Coauthors, 2017: Extended Reconstructed Sea Surface Temperature, Version 5 (ERSSTv5): Upgrades, Validations, and Intercomparisons. *Journal of Climate*, **30**, 8179–8205, https://doi.org/10.1175/JCLI-D-16-0836.1.

Huang, G., K. Hu, and S.-P. Xie, 2010: Strengthening of Tropical Indian Ocean Teleconnection to the Northwest Pacific since the Mid-1970s: An Atmospheric GCM Study*. *Journal of Climate*, **23**, 5294–5304, https://doi.org/10.1175/2010JCLI3577.1.

——, X. Qu, and K. Hu, 2011: The impact of the tropical Indian Ocean on South Asian High in boreal summer. *Adv. Atmos. Sci.*, **28**, 421–432, https://doi.org/10.1007/s00376-010-9224-y.

Huang, P., and J. Ying, 2015: A Multimodel Ensemble Pattern Regression Method to Correct the Tropical Pacific SST Change Patterns under Global Warming. *Journal of Climate*, **28**, 4706–4723, https://doi.org/10.1175/JCLI-D-14-00833.1.

Jiang, W., G. Huang, K. Hu, R. Wu, H. Gong, X. Chen, and W. Tao, 2017: Diverse relationship between ENSO and the Northwest Pacific summer climate among CMIP5

Accepted for publication in *Journal of Climate*. DOI 10.1175/JCLI-D-25-0438.1.

models: dependence on the ENSO decay pace. *Journal of Climate*, **30**, 109–127, https://doi.org/10.1175/jcli-d-16-0365.1.

——, ——, P. Huang, and K. Hu, 2018: Weakening of Northwest Pacific anticyclone anomalies during post-El Niño summers under global warming. *Journal of Climate*, **31**, 3539–3555, https://doi.org/10.1175/jcli-d-17-0613.1.

——, ——, ——, R. Wu, K. Hu, and W. Chen, 2019: Northwest Pacific anticyclonic anomalies during post-El Niño summers determined by the pace of El Niño decay. *Journal of Climate*, **32**, 3487–3503, https://doi.org/10.1175/jcli-d-18-0793.1.

——, P. Huang, G. Li, and G. Huang, 2020: Emergent constraint on the frequency of central Pacific El Niño under global warming by the equatorial Pacific cold tongue bias in CMIP5/6 models. *Geophysical Research Letters*, **47**, https://doi.org/10.1029/2020gl089519.

——, ——, G. Huang, and J. Ying, 2021: Origins of the Excessive Westward Extension of ENSO SST Simulated in CMIP5 and CMIP6 Models. *Journal of Climate*, **34**, 2839–2851, https://doi.org/10.1175/jcli-d-20-0551.1.

——, H. Gong, P. Huang, L. Wang, G. Huang, and L. Hu, 2022: Biases and improvements of the ENSO-East Asian winter monsoon teleconnection in CMIP5 and CMIP6 models. *Clim Dyn*, **59**, 2467–2480, https://doi.org/10.1007/s00382-022-06220-5.

Kalnay, E., and Coauthors, 1996: The NCEP/NCAR 40-year reanalysis project. *Bulletin of the American Meteorological Society*, **77**, 437–471, https://doi.org/10.1175/1520-0477(1996)077%253C0437:tnyrp%253E2.0.co;2.

Klein, S. A., B. J. Soden, and N. C. Lau, 1999: Remote sea surface temperature variations during ENSO: Evidence for a tropical atmospheric bridge. *Journal of Climate*, **12**, 917–932, https://doi.org/10.1175/1520-0442(1999)012%253C0917:rsstvd%253E2.0.co;2.

Lau, N. C., and M. J. Nath, 1996: The role of the "'atmospheric bridge'" in linking tropical Pacific ENSO events to extratropical SST anomalies. *Journal of Climate*, **9**, 2036–2057, https://doi.org/10.1175/1520-0442(1996)009%253C2036:trotbi%253E2.0.co;2.

——, and ——, 2003: Atmosphere-ocean variations in the Indo-Pacific sector during ENSO episodes. *Journal of Climate*, **16**, 3–20, https://doi.org/10.1175/1520-0442(2003)016%253C0003:aoviti%253E2.0.co;2.

Li, G., S.-P. Xie, and Y. Du, 2015: Climate Model Errors over the South Indian Ocean Thermocline Dome and Their Effect on the Basin Mode of Interannual Variability. *Journal of Climate*, **28**, 3093–3098, https://doi.org/10.1175/JCLI-D-14-00810.1.

——, ——, C. He, and Z. Chen, 2017: Western Pacific emergent constraint lowers projected increase in Indian summer monsoon rainfall. *Nature Clim Change*, **7**, 708–712, https://doi.org/10.1038/nclimate3387.

Liu, S., S. V. Raghavan, B. J. Ona, and N. S. Nguyen, 2023: Bias evaluation in rainfall over Southeast Asia in CMIP6 models. *Journal of Hydrology*, **621**, 129593, https://doi.org/10.1016/j.jhydrol.2023.129593.

Accepted for publication in *Journal of Climate*. DOI 10.1175/JCLI-D-25-0438.1.

Long, S.-M., G. Li, K. Hu, and J. Ying, 2020: Origins of the IOD-like Biases in CMIP Multimodel Ensembles: The Atmospheric Component and Ocean–Atmosphere Coupling. *Journal of Climate*, **33**, 10437–10453, https://doi.org/10.1175/JCLI-D-20-0459.1.

Masumoto, Y., and G. Meyers, 1998: Forced Rossby waves in the southern tropical Indian Ocean. *Journal of Geophysical Research-Oceans*, **103**, 27589–27602, https://doi.org/10.1029/98jc02546.

McKenna, S., A. Santoso, A. Sen Gupta, and A. S. Taschetto, 2024: Understanding Biases in Indian Ocean Seasonal SST in CMIP6 Models. *JGR Oceans*, **129**, e2023JC020330, https://doi.org/10.1029/2023JC020330.

North, G. R., T. L. Bell, R. F. Cahalan, and F. J. Moeng, 1982: Sampling Errors in the Estimation of Empirical Orthogonal Functions. *Mon. Wea. Rev.*, **110**, 699–706, https://doi.org/10.1175/1520-0493(1982)110%253C0699:SEITEO%253E2.0.CO;2.

Power, S. B., F. Delage, R. Colman, and A. Moise, 2012: Consensus on twenty-first-century rainfall projections in climate models more widespread than previously thought. *Journal of Climate*, **25**, 3792–3809, https://doi.org/10.1175/jcli-d-11-00354.1.

Qu, X., and G. Huang, 2012a: An Enhanced Influence of Tropical Indian Ocean on the South Asia High after the Late 1970s. *Journal of Climate*, **25**, 6930–6941, https://doi.org/10.1175/JCLI-D-11-00696.1.

——, and ——, 2012b: Impacts of tropical Indian Ocean SST on the meridional displacement of East Asian jet in boreal summer. *Intl Journal of Climatology*, **32**, 2073–2080, https://doi.org/10.1002/joc.2378.

Schott, F. A., S. Xie, and J. P. McCreary, 2009: Indian Ocean circulation and climate variability. *Reviews of Geophysics*, **47**, 2007RG000245, https://doi.org/10.1029/2007RG000245.

Tao, W., G. Huang, K. Hu, H. Gong, G. Wen, and L. Liu, 2016: A study of biases in simulation of the Indian Ocean basin mode and its capacitor effect in CMIP3/CMIP5 models. *Clim Dyn*, **46**, 205–226, https://doi.org/10.1007/s00382-015-2579-0.

——, ——, R. Wu, K. Hu, P. Wang, and H. Gong, 2018: Origins of Biases in CMIP5 Models Simulating Northwest Pacific Summertime Atmospheric Circulation Anomalies during the Decaying Phase of ENSO. *Journal of Climate*, **31**, 5707–5729, https://doi.org/10.1175/jcli-d-17-0289.1.

Tao, W. C., G. Huang, K. M. Hu, X. Qu, G. H. Wen, and H. N. Gong, 2015: Interdecadal modulation of ENSO teleconnections to the Indian Ocean Basin Mode and their relationship under global warming in CMIP5 models. *International Journal of Climatology*, **35**, 391–407, https://doi.org/10.1002/joc.3987.

Taylor, K. E., R. J. Stouffer, and G. A. Meehl, 2012: An overview of CMIP5 and the experiment design. *Bulletin of the American Meteorological Society*, **93**, 485–498, https://doi.org/10.1175/bams-d-11-00094.1.

Accepted for publication in *Journal of Climate*. DOI 10.1175/JCLI-D-25-0438.1.

Weller, E., and W. Cai, 2013: Realism of the Indian Ocean Dipole in CMIP5 Models: The Implications for Climate Projections. *Journal of Climate*, **26**, 6649–6659, https://doi.org/10.1175/JCLI-D-12-00807.1.

Wu, R., B. P. Kirtman, and V. Krishnamurthy, 2008: An asymmetric mode of tropical Indian Ocean rainfall variability in boreal spring. *Journal of Geophysical Research-Atmospheres*, **113**, https://doi.org/10.1029/2007jd009316.

Xie, S. P., H. Annamalai, F. A. Schott, and J. P. McCreary, 2002: Structure and mechanisms of South Indian Ocean climate variability. *Journal of Climate*, **15**, 864–878, https://doi.org/10.1175/1520-0442(2002)015%253C0864:samosi%253E2.0.co;2.

——, Y. Kosaka, Y. Du, K. M. Hu, J. Chowdary, and G. Huang, 2016: Indo-western Pacific ocean capacitor and coherent climate anomalies in post-ENSO summer: A review. *Adv. Atmos. Sci.*, **33**, 411–432, https://doi.org/10.1007/s00376-015-5192-6.

Xie, S.-P., K. Hu, J. Hafner, H. Tokinaga, Y. Du, G. Huang, and T. Sampe, 2009: Indian Ocean Capacitor Effect on Indo-Western Pacific Climate during the Summer following El Niño. *Journal of Climate*, **22**, 730–747, https://doi.org/10.1175/2008jcli2544.1.

Yang, J. L., Q. Y. Liu, S. P. Xie, Z. Y. Liu, and L. X. Wu, 2007: Impact of the Indian Ocean SST basin mode on the Asian summer monsoon. *Geophysical Research Letters*, **34**, 5, https://doi.org/10.1029/2006gl028571.

——, ——, and Z. Y. Liu, 2010: Linking Observations of the Asian Monsoon to the Indian Ocean SST: Possible Roles of Indian Ocean Basin Mode and Dipole Mode. *Journal of Climate*, **23**, 5889–5902, https://doi.org/10.1175/2010jcli2962.1.

Zheng, X.-T., S.-P. Xie, and Q. Liu, 2011: Response of the Indian Ocean Basin Mode and Its Capacitor Effect to Global Warming. *Journal of Climate*, **24**, 6146–6164, https://doi.org/10.1175/2011jcli4169.1.

——, L. Gao, G. Li, and Y. Du, 2016: The Southwest Indian Ocean thermocline dome in CMIP5 models: Historical simulation and future projection. *Advances in Atmospheric Sciences*, **33**, 489–503, https://doi.org/10.1007/s00376-015-5076-9.

Zhou, S., P. Huang, G. Huang, and K. Hu, 2019: Leading source and constraint on the systematic spread of the changes in East Asian and western North Pacific summer monsoon. *Environmental Research Letters*, **14**, https://doi.org/10.1088/1748-9326/ab547c.

——, G. Huang, and P. Huang, 2020: Inter-model Spread of the Changes in the East Asian Summer Monsoon System in CMIP5/6 Models. *JGR Atmospheres*, **125**, 2020JD033016, https://doi.org/10.1029/2020JD033016.

Accepted for publication in *Journal of Climate*. DOI 10.1175/JCLI-D-25-0438.1.